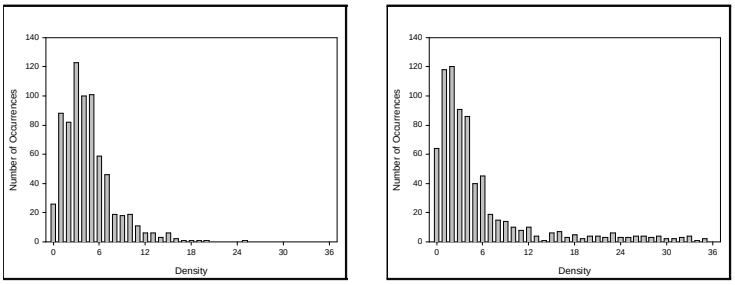

(a) H=18 Vertical $\bar{\rho}$=10/72 (b) H=18 Vertical $\bar{\rho}$=12/72
Figure 5.42 Column density histograms at $T = 0.8$ for $H = 18$

5.3.6. Co-existence Curves

The estimates for the co-existence curves for systems with SPBC, using a variety of densities and temperatures, are given in Figure 5.43. The error bars in Figure 5.43 reflect uncertainties due to the step size in either $\bar{\rho}$ or T, as well as the short time scales of our runs (20K MCS). As a reminder, we selected these parameters to limit the study within our resources *and* to produce a "first approximation" (i.e., 10% accuracy) of co-existence curves. To arrive at better estimates, we need to have larger system sizes and longer runs. Our use of many methods, mostly showing points which lie within the error bars of each other, allows us to make several conclusions. The $H = 3$ co-existence curve (Figure 5.43a) lies "within" the PBC curve shown in Figure 5.17. Likewise, the $H = 4$ curve(Figure 5.43b) lies within the $H = 3$ curve. In both of these cases, the order state is a single forward tilting strip. Even for low densities, the strip is a system spanning type. Further more, these narrow strips drift around the torus, unlike the PBC case.

For higher shifts, the trend is reversed: the $H = 9$ curve (Figure 5.43c) lies somewhat within the $H = 18$ curve (Figure 5.43d). However, we should note that the ordered states are actually not the same. Both display mainly the multiply wound strip variety, though systems with high density have size spanning strips with different Ω. At lower densities, the inhomogeneities take the form of a drifting droplet, which is clearly a more complicated structure.

There is a difference between the co-existence curves, using the two methods (Figure 4.6a vs Figure 5.17), for the system with PBC. We believe this is due to finite size effects. In any case, both methods give us strips aligned with the field so that no uniform drifting occurs. However, for systems with $H = 3, 4$, the strips in low density cases drift, with speeds decreasing with increasing width. At , $\bar{\rho} = 1/2$, drifting stops. Thus, it may be difficult to argue that the ordered states for half-filled systems are the same as those at other densities and that

the two methods perhaps measure *two distinct* co-existence curves. On the other hand, comparing the results from these two methods (Figure 4.6b vs Figure 5.43a and Figure 4.6c vs Figure 5.43b), we see that differences are no greater than in the PBC case. By contrast, the difference is significantly greater for the system with high shifts (Figure 4.6d,e vs 5.43c,d). As mentioned above, this may be traced to the drastically different ordered states, with drifting droplets vs. wandering multistrips. It is clear that only further investigations can lead to better understanding of these co-existence curves.

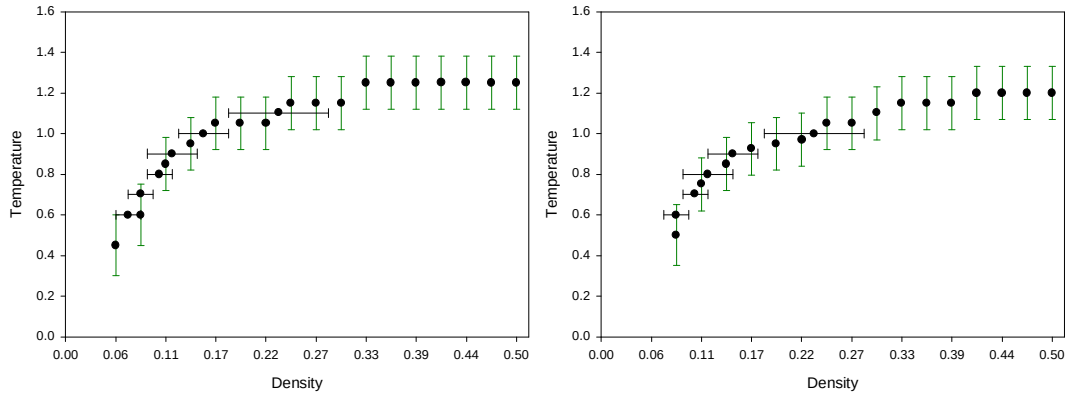

(a) H=3 (b) H=4

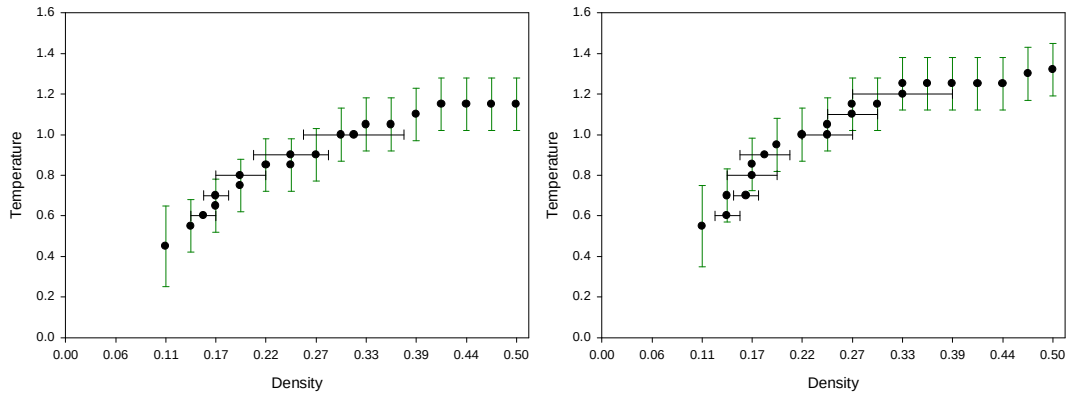

(c) H=9 (d) H=18

Figure 5.43 Co-existence curves for the SPBC systems

6. Co-existence of a System with Large Fluctuations

In Chapters 4 and 5, we established the co-existence curves for SPBC with low shifts $H = 0, 3, 4$ and high shifts $H = 9, 18$. Because of certain peculiarities in the $H = 6$ case, we have reserved discussing this midsize shift until now. We use both of the methods described in Chapters 4 and 5 above for estimating the H=6 co-existence curve. For brevity, we will refer to these as Method I and Method II, respectively. Unless otherwise noted, all simulations begin with a single strip tilted in accordance with the shift.

6.1. Method I

At half density, the richness of the H=6 can be seen easily by looking at sample configurations. The configurations in Figure 6.1 illustrates typical behavior in the *heating* cycle. At temperatures below $T = 0.8$, such as that shown in Figure 6.1a, the favored state displays a multiply wound strip with a *backward* tilt: $\tan\theta = -2/36$! This tilt is better seen when the configuration is displayed larger (Figure D.1 in Appendix D). By the time the temperature reaches 0.8, shown in Figure 6.1b, the favored bulk state appears to be *combination* of a single strip with $\tan\theta = 6/36$ and long strand of back tilted cluster. This "*hybrid*" state is similar to the configuration shown in Figure 4.4d, where it was used to help explain the large density deviations for the $H = 9$ system when $T \geq 1.0$. However, for $H = 6$, we see the hybrid state for temperatures as low as $T = 0.8$. The configurations in this state appear to be a single bulk cluster, with a tilt dictated by the SPBC, "boiling off" particles which re-cluster into a thin "icicle". This icicle often occurs with a backward tilt. Since icicles have varying lengths, we will classify clusters with *no* icicle - a single forward tilted strip- into this "hybrid" category. Indeed, such a large strip often becomes the source for the icicles. Above $T = 0.8$, the configurations remains in the *hybrid* state until the system disorders at $T \sim 1.2$.

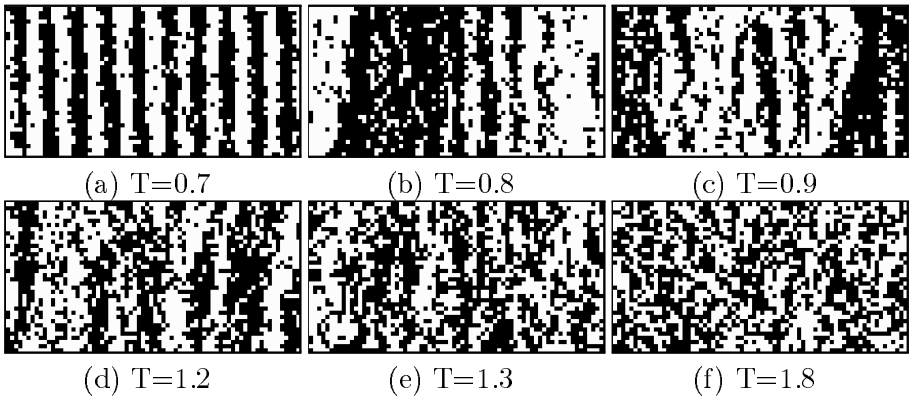

(a) T=0.7 (b) T=0.8 (c) T=0.9

(d) T=1.2 (e) T=1.3 (f) T=1.8

Figure 6.1 Typical configurations in the heating cycle for $H = 6$, $\bar{\rho} = 36/72$

For Method I, the densities of the cluster are used to estimate the co-existence curve. We would expect, as with the high shift systems, that the compact clusters would give a less volatile estimate than the rarified. Table 6.1 lists the cluster sizes and densities for the heating and cooling cycles. As explained in Chapter 4, the estimates of cluster sizes and densities include the hole clusters. At temperatures below $T = 1.0$, the cluster size on the heating and cooling cycles are within the error bars of each other. At $T = 1.0$ and $T = 1.1$ the results are not as consistent. However, the density estimates are similar at temperatures down to $T = 0.8$. Below that point, there are inconsistencies leading to a large uncertainty in the average density. Being poor estimates, they are left out of the table below and not used in constructing the co-existence curve. Only the densities from higher temperatures are used. A plot of the curve is shown along with the Method II estimate at the end of this chapter (Figure 6.14a).

Table 6.1 Cluster Size and Density Estimates for H=6

Temp\ Shift	Cluster Size H=6			Cluster Densities H=6		
	heating	cooling	V_{clus}	heating	cooling	ρ
T=0.5	1294±3	1291±12	1293±9	0.4±0.1	1.3±0.9	-
T=0.6	1293±5	1287±19	1291±13	0.5±0.2	2.7±0.4	-
T=0.7	1229±195	1257±53	1240±156	0.8±0.2	4.1±2.7	-
T=0.8	1270±62	1277±46	1273±49	8.6±2.0	5.8±3.0	6.5±2.5
T=0.9	1094±333	801±158	900±279	10.9±4.0	7.1±3.5	8.4±3.7
T=1.0	606±102	876±324	742±272	13.3±4.9	10.4±3.7	11.9±4.5
T=1.1	856±296	595±185	709±270	16.4±7.0	14.9±4.5	15.6±5.7

The density estimates from the *cooling* cycle are smoother as a function of temperature. We do not fully understand this phenomenon: that the hybrid state is more "stable" on cooling, even for temperatures below $T = 0.8$. Some configurations for this cycle are shown in Figure 6.2. It is reasonable to conclude that order sets in at $T \sim 1.2$. Figure 6.2b show a rarified hybrid state that shows strips with both forward and backward tilt. In contrast, Figure 6.2c shows a configuration with only forward strips. The large strip has a very rough and wide evaporating (right) edge which appears to be producing an icicle. Particles from this large strip feed a smaller, forward tilting, strip. The contrast between Figures 6.2b and 6.2c is a good illustration of the extraordinary nature of the large fluctuations in the $H = 6$ system. Icicles can grow and shrink, as well as break off to forming thin strips. Of course, due to the SPBC, all strips drift, leading to their coalescence.

Unlike in the heating cycle, the hybrid state persists even at $T = 0.6$. Below that, the system develops into a multi-strip state with nontrivial winding (Figures 6.2f). By contrast, such states are stable up to $T = 0.7$ during the heating. This phenomenon of hysteresis, as well as the role of metastability, will be further investigated in the two sections below.

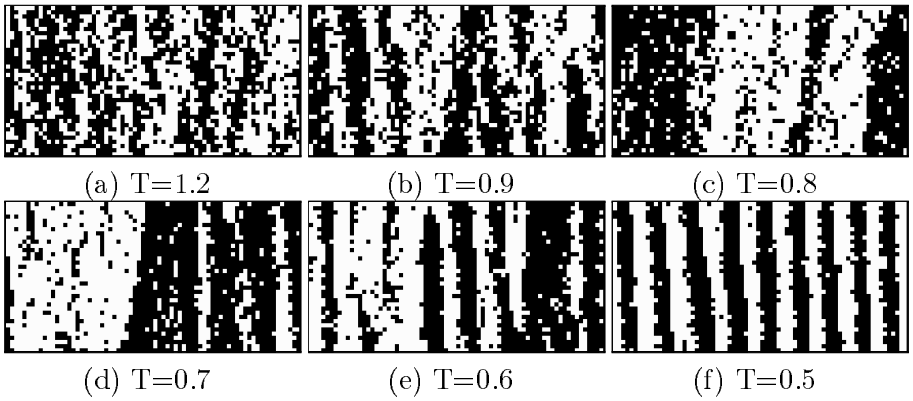

Figure 6.2 Typical configurations in the cooling cycle for $H = 6$, $\bar{\rho} = 36/72$

6.2. Method II

This approach to an estimate of the co-existence curve is described in detail in Chapter 5. In this section, we first present sample configurations for a system with a low system density. To be consistent with Chapter 5, we include a more detailed description of the $\bar{\rho} = 8/72$ system. Next we discuss the order parameters

for both systems ($\bar{\rho} = 36/72, 8/72$). Other system densities are then described in order to further explain the behavior of two ordered states. Also, as in Chapter 5, a study with constant temperature but varying $\bar{\rho}$ is carried out. This section ends by showing the estimated co-existence curves for H=6.

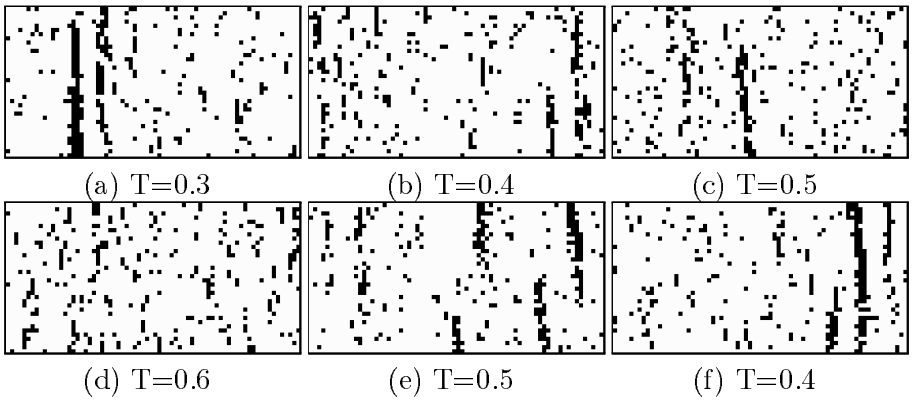

Figure 6.3 Typical configurations for $\bar{\rho} = 8/72$

The configurations in Figure 6.3 show sample configurations from the heating and cooling cycles for the $\bar{\rho}$=8/72 system. Notice that all the clusters in the low temperature states (Figures 6.4a,f) display the backward tilt. In contrast, clusters in the $H = 3, 4$ cases show forward tilt, while they are aligned vertically for systems with large shifts ($H = 9, 18$). By inspection alone, we might identify the transition as $T = 0.50 \pm .05$., where a single large cluster first appear. However, as we will show, all the order parameters estimate the transition temperature to be lower by another 0.1. This highlights one of the difficulties in determining order in finite systems with low density and high shifts ($H \geq 6$). The multiple winding tends to allow the creation of multiple small strips that later join to form a larger strip. Further study is needed for developing a systematic criteria for establishing whether a cluster is sufficiently large to warrant characterizing a system as "ordered". Here, as a first approximation for co-existence, we limit ourselves to using the crude order parameters introduced in Chapter 5.

Figures 6.4 shows the internal energy for the $\bar{\rho} = 36/72$ and $\bar{\rho} = 8/72$ cases. Compared to the other SPBC systems, these are similar for the half-filled system. For the low density case, there is some hysteresis, resembling the $H = 9$ case (Figure 5.34b) more than the low shift ones, which display clear discontinuities. In this aspect, it is possible that the $H = 9$ system is also one with exceptionally large fluctuations.

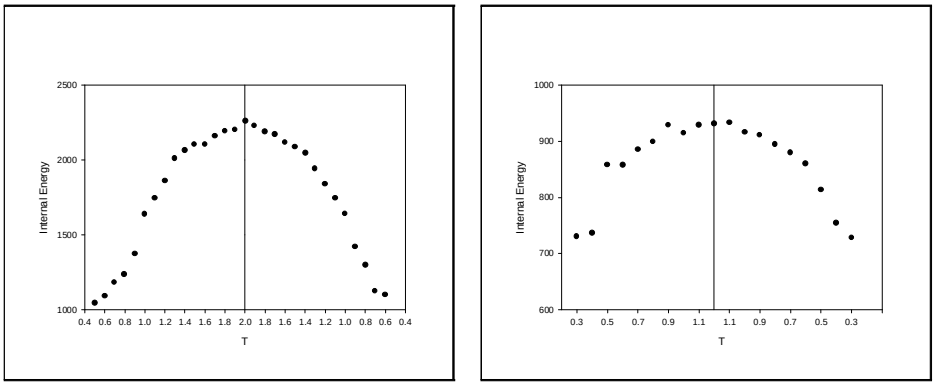

(a) $\bar{\rho}$=36/72 (b) $\bar{\rho}$=8/72

Figure 6.4 Internal energy vs. temperaturefor $\bar{\rho} = 36/72$ and $\bar{\rho} = 8/72$ systems.

Figures 6.5 show the average cluster sizes for the two systems as a function of T during the heating and cooling cycles. Using this measure, the half-filled system behaves more similar to the *low* shift cases, as the function display no sizable discontinuity. For the low desnity system, the discontinuity is clear, as in all the other SPBC systems, so that we are tempted to assign a clear transition temperature, based on cluster sizes alone. However, as we will see, the behavior of this $H = 6$ system is quite complex in the $\bar{\rho}$-T plane. Only at sufficiently low densities is the transition clearly into a state with one or two large clusters of the same type ($\tan\theta < 0$). At higher densities, two transitions (in T) seem a more appropriate description. We should mention that, with densities less than 6/72, all the observations show only homogeneous states.

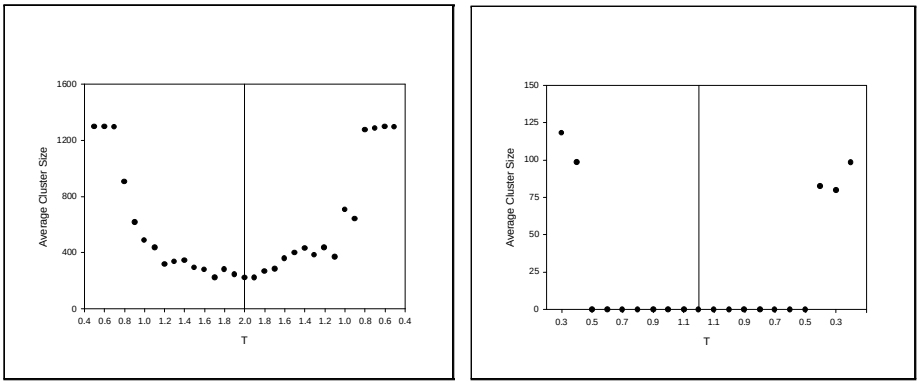

(a) $\bar{\rho}$=36/72 (b) $\bar{\rho}$=8/72

Figure 6.5 Average cluster size vs. temperature for $\bar{\rho} = 36/72$ and $\bar{\rho} = 8/72$ systems.

Next, we turn to some details of the histograms for the column densities in the case of $\rho = 36/72$. Each plot in Figure 6.6 shows two histograms. The vertical bars are associated with ρ_{-2}, the skewed column density with $\tan\theta = -2/72$. By contrast, the line plots ρ_6, the column density with $\tan\theta = 6/72$. Figure 6.7a shows clearly phase separation according to ρ_{-2}. Yet, according to ρ_6 the system is naively disordered! This contrast highlights the difficulties in identifying ordered states properly, since a single multiply-wound, backward- tilting ($\Omega = 9$) strip can appear "random" to ρ_6. Had there been a large single strip with $\Omega = 0$, we would have phase separation in ρ_6 instead!

For $T \geq 0.8$, the two column densities are distributed similarly. At $T = 0.9$, the two column densities resemble a uniform distribution! Comparing this to the distribution of a system near total disorder ($T = 1.8$), we emphasize that a flat distribution is an exceedingly unusal phenomenon. When we examine the configurations (e.g., Fig. 6.1c or 6.2b), we see the origin. There are regions of the system clearly in the $\Omega = 9$ state and others in the $\Omega = 0$ state. Thus, it is possible that the histograms in Fig. 6.6c are comprised of phase separated, bi-modal, components, as well as single peaked "random" components. Clearly, a study with $L > 72$ will be most helpful in testing this hypothesis. At this stage, we simply refer to this extraordinary state as the "hybrid" state. As T increases, the distribution appears more Gaussian and we may identify the systems as being disordered for $T \geq 1.2$.

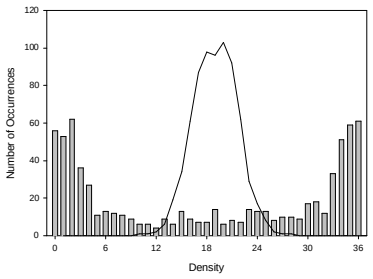

(a) T=0.7

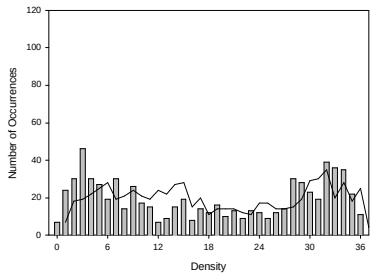

(b) T=0.8

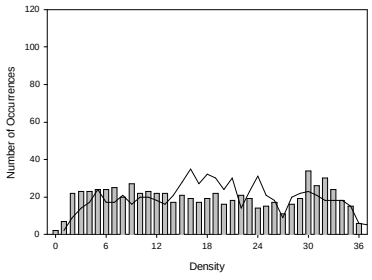

(c) T=0.9

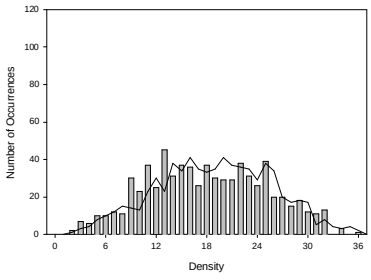

(d) T=1.2

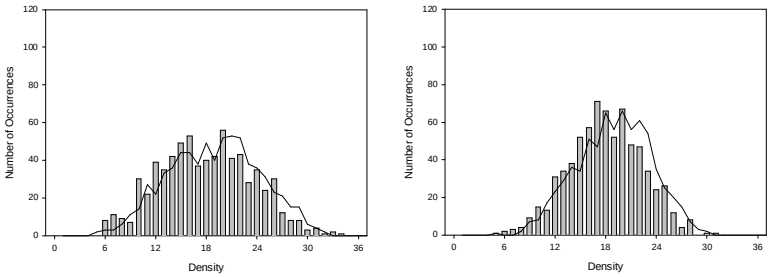

(e) T=1.3 (e) T=1.8

Figure 6.6 Histograms of ρ_{-2} (bars) and ρ_6 (line) for a half-filled $H = 6$ system.

Not surprisingly, when we characterize these distributions with single numbers like $\Delta\rho_{-2}$ and $\Delta\rho_6$, the two are essentially the same except when for the $\Omega = 8$ states. Therefore, they are useful for distinguishing the multi-stripped states from the other two: hybrid and disordered. Figure 6.7 shows these widths as a function of temperature for both the $\bar{\rho} = 36/72$ and $\bar{\rho} = 8/72$ systems, with the dots and the line representing $\Delta\rho_{-2}$ and $\Delta\rho_6$, respectively. For the less dense system, the distinction between the widths are not as clear for the $\Omega = 9$ states. To some extent, since this system contains a "droplet" (i.e., a cluster which does not span the system, as in Fig. 6.3a,f) which is tilted backwards, considerable weight for ρ_6 comes from the homogeneous region, leading to a less clear picture for $\Delta\rho_6$. For the low density system, as we pointed out above, there seems to be no hybrid states.

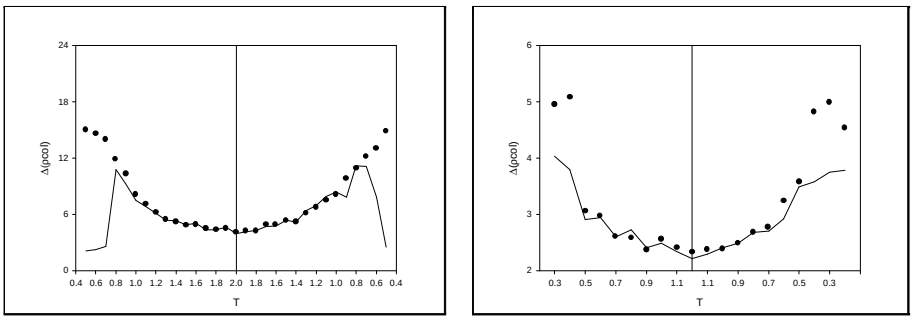

(a) $\bar{\rho}$=36/72 (b) $\bar{\rho}$=8/72

Figure 6.7 The widths $\Delta\rho_h$ vs. T for the $\bar{\rho} = 36/72$ and $\bar{\rho} = 8/72$ systems.

Structure factors are also used to detect ordering. Since there is a large variety of orientations for the strips, we focused only on the ordinary S and the sum of

the intensities in the first 10 wave numbers: $< P_0 >$. Figure 6.8 shows combined plots of the intensity sum $< P_0 >$ and the structure factor $S(1,0)$ as a function of T. Observe that $S(1,0)$ is somewhat sensitive to the presence of a single strip, which occurs frequently in the hybrid state. On the other hand, $< P_0 >$ measures ordering into a variety of strip widths. Thus, the behavior of these two order parameters are similar to $\Delta\rho_h$.

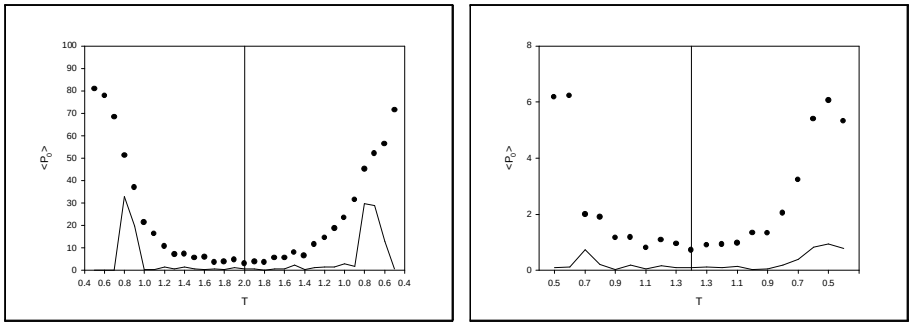

(a) $\bar{\rho}$=36/72 (b) $\bar{\rho}$=8/72

Figure 6.8 $< P_0 >$ and $S(1,0)$, shown as dots and a line respectively

Using these sets of order parameters to establish the transition temperature for system at other densities $6/72 \leq \bar{\rho} \leq 36/72$. The transition temperatures are plotted in Figure 6.13b, with vertical uncertainty bars. As mentioned in the previous chapter, the uncertainty comes from the coarseness of the temperature steps and the slight discrepancies in measuring order parameters.

As explained in Chapter 5, this approach also relies on studying the system at constant temperature and varying $\bar{\rho}$. This not only helps to establish the coexistence curve better, but also to determine the boundary between the two types of ordering (hybrid vs strips). Seven temperatures were selected: $0.5 \leq T \leq 1.1$ in 0.1 increments. As with the studies in the previous chapter, the system is initialized in a disorder state with $\bar{\rho} = 4/72$. After evolving for 20K MCS, measurements were taken and then 72 particles are randomly added to increase the system density. The procedure is repeated until $\bar{\rho} = 36/72$, held for an additional 20 K MCS, and then reversed, by stepping the density back down to $\bar{\rho} = 4/72$. These density-increasing and decreasing cycles are analogous to the heating and cooling cycles. Figures 6.9-12 show typical configurations at three densities, for $0.5 \leq T \leq 0.8$.

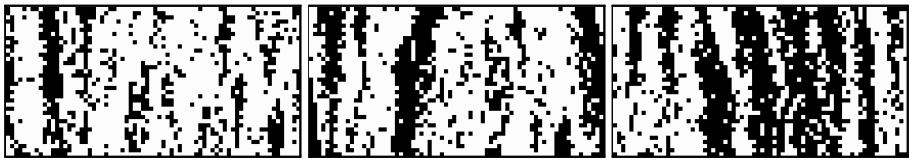

(a) $\bar{\rho}$=20/72 (b) $\bar{\rho}$=26/72 (c) $\bar{\rho}$= 36/72

Figure 6.9 Typical configurations for three $\bar{\rho}$'s at fixed $T = 0.8$

(a) $\bar{\rho}$=20/72 (b) $\bar{\rho}$=26/72 (c) $\bar{\rho}$=36/72

Figure 6.10 Typical configurations for three $\bar{\rho}$'s at fixed $T = 0.7$

(a) $\bar{\rho}$=20/72 (b) $\bar{\rho}$=26/72 (c) $\bar{\rho}$=36/72

Figure 6.11 Typical configurations for three $\bar{\rho}$'s at fixed $T = 0.6$

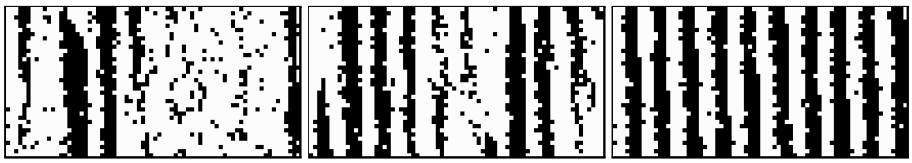

(a) $\bar{\rho}$=20/72 (b) $\bar{\rho}$=26/72 (c) $\bar{\rho}$=36/72

Figure 6.12 Typical configurations for three $\bar{\rho}$'s at fixed $T = 0.5$

As observed by using Method I, system with small densities tend to display clusters with $\tan\theta \approx -2/36$. As $\bar{\rho}$ is increased, a hybrid state gradually sets in. For example, in Fig 6.9b, both forward and backward tilted strips are seen. At the highest density (half-filled), the hybrid nature is most evident. It is arguable whether there is a large vertical strip which is made up of thinner ones with negative θ. At the lower temperatures, the less dense systems are dominated by one or two long clusters which wind around the torus several times due to the SPBC. All appear to have $\tan\theta \simeq -2/36$. See, e.g., Figs 6.10-11 (a) and (b). On the other hand, the half filled system remains in a hybrid state (Figures 6.9c-11c) until the lower temperature of $T = 0.5$.

As in Chapter 5, $\Delta\rho_h$ is used as an order parameter to determine at what $\bar{\rho}$ the system orders. These estimated $\bar{\rho}$'s, along with T, are used to estimate the

co-existence curve. These values are plotted in Figure 6.13b with horizontal error bars. The uncertainties include the coarseness of the density steps. Note that, for the higher temperatures, the uncertainties are necessarily large since changing $\bar{\rho}$ corresponds to approaching the co-existence curve tangentially. In this plot, we have restricted ourselves to the boundary between a homogeneous phase, which we label as disorder, and a state with some inhomogeneity, whether that is in the form of large clusters, fully formed strips, or hybrids.

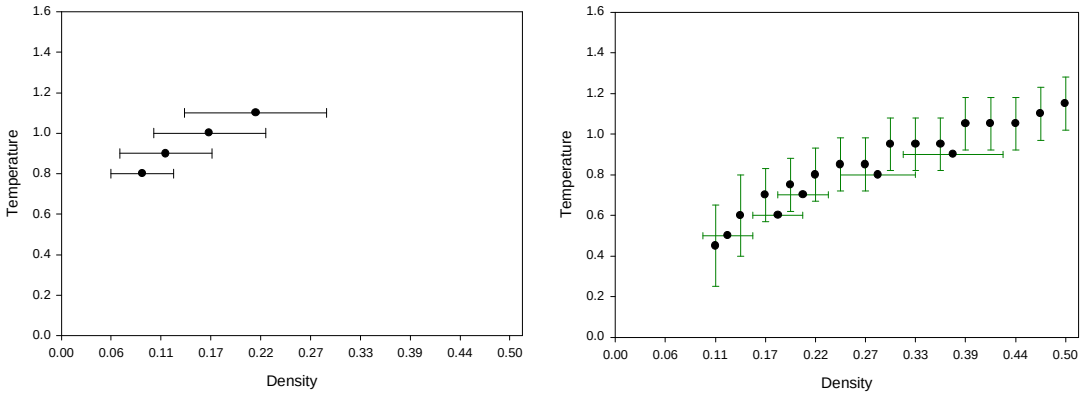

(a) Method I

(b) Method II

Figure 6.13 Co-existence curve estimates for $H = 6$

In the next plot (Figure 6.14), we attempt to show the boundary between a hybrid state and a "pure" one. In the latter, we have mainly clusters of *negative* multiple winding, i.e., backward tilting strips. For low densities, these clusters do not span the system and may be referred to as "droplets". Unlike the equilibrium droplet, however, we expect these to drift and/or breakup, so that many more simulations are needed before we can arrive at a clear picture of their nature.

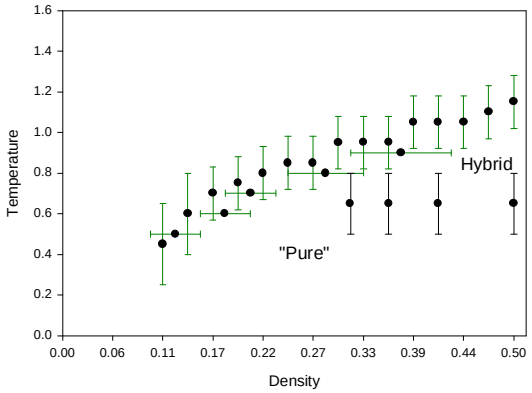

Figure 6.14 Boundary between hybrid and "pure" states.

6.3. Metastable States

To end this chapter, we devote this section to a study with longer runs at $T = 0.5, 0.7$, and 0.8, in order to explore the distinction between hybrid and pure states further. In particular, we study time traces of several widths for the half-filled system, starting with *different initial configurations*. As a result, the phenomenon of metastability is more clearly displayed. In the following, traces for only $\Delta\rho_{-2}$ and $\Delta\rho_6$ are shown. Finally, time traces for two other systems: $\bar{\rho} = 26/72$ and $20/72$ will also be shown. For these plots, runs of 250K MCS are used, while measurements are taken every 200 MCS within the following intervals [20-40], [60-80], ... [220-240] (in K MCS from the beginning).

For Figures 6.15a,b, the initial conditions are, respectively, completely ordered states with multistrips and single strip. The former would be a state with $\Omega = 9$, i.e., nine strips with a backward tilt of $\tan\theta = -2/36$. Thus, the distribution for ρ_{-2} is maximally phase separated, with full weights at 0 and 36. So, $\Delta\rho_{-2} = 18$ initially. A configuration like Figure 6.12c will produce a large value for this width. By contrast, these states give rise to low values for $\Delta\rho_6$, as evident from the histogram Figure 6.6a. For the completely ordered state with a single, forward tilting, strip (of width 36), ρ_6 is maximally phase separated, so that $\Delta\rho_6 = 18$. As the system evolves toward a hybrid structure, both $\Delta\rho_6$ and $\Delta\rho_{-2}$ will converge, as in the histogram Figure 6.6c.From Figures 6.15 we see that, for $T = 0.8$, the final steady state is hybrid regardless of initial conditions. It is interesting that, starting with the multistrip state, the system appears to become hybrid like for the first 40K MCS or so, settles back into a multistrip state for another 50K

MCS before arriving at the final state near 150K MCS. These long life times are obstacles for studies with short runs and help explain the hysteresis observed in Method I. In the heating cycle, the system starts at a very low temperature and settles into multi-stripped state. As the temperature increases to as high as 0.8, the system remains in this state, even though the hybrid is the final steady state. The short evolution times (20K MCS) allows our system to remain in this metastable, multi-stripped state. By contrast, during the cooling cycle, the system finds itself in the hybrid, metastable state even down to $T = 0.6$.

Figures 6.16 and 6.17 show similar traces at lower temperatures. For the $T = 0.7$ system, the final states display much larger fluctuations than for the $T = 0.8$ case, while the multistrip initial state appears to be more resilient. However, the life time of this initial state is similar to that for the $T = 0.8$ case. Comparing this figure with the one for $T = 0.8$, we would conclude that this temperature setting is closer to the boundary between hybrid and multistripped states. In contrast, for the $T = 0.5$ system, regardless of the initial conditions, the final state is multi-stripped, as so cleanly displayed in Figures 6.17. It is curious that there are some serious fluctuations at the early stages (up to 80K MCS) in Figure 6.17a even with an initial configuration belonging to the steady state. If such behavior persists in future runs, it would pose another challenge to the understanding of the dynamic, co-operative properties in such systems.

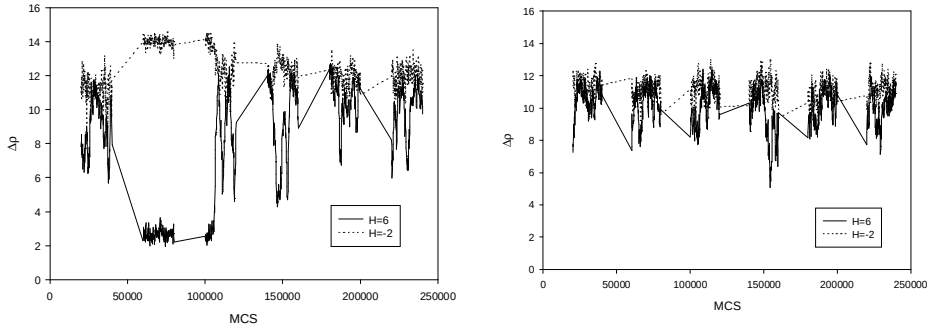

(a) (b)

Figure 6.15 Time traces of $\Delta\rho_6$ and $\Delta\rho_{-2}$ for $\bar{\rho} = 36/72$ at $T = 0.8$

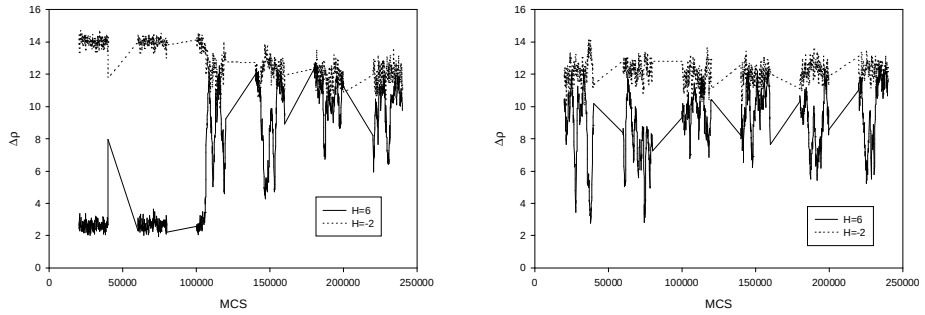

(a) (b)

Figure 6.16 Time traces of $\Delta\rho_6$ and $\Delta\rho_{-2}$ for $\bar{\rho} = 36/72$ at $T = 0.7$

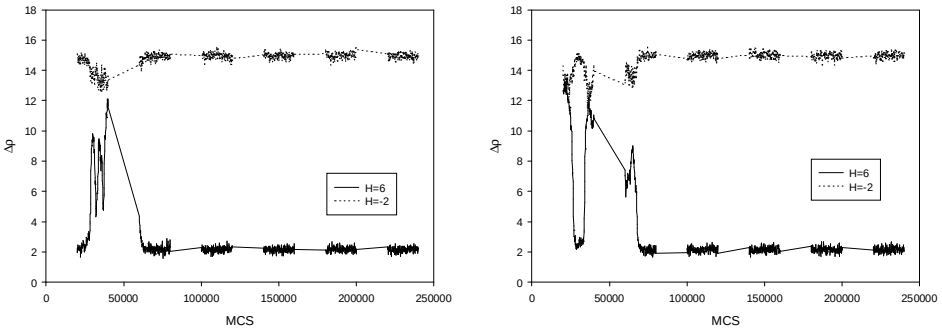

(a) (b)

Figure 6.17 Time traces of $\Delta\rho_6$ and $\Delta\rho_{-2}$ for $\bar{\rho} = 36/72$ at $T = 0.5$

Although we are as yet to develop a clear picture for the nature of this hybrid state, we tentatively suggest the following. For the half-filled system, both interfaces of a single, forward tilted, strip are unstable against the drive. Thus, the drive would favor a strip with multiple winding, so as to make interfaces as vertical as possible. With small shifts, such a state will contain a large number of narrow strips. On the other hand, the interparticle attraction favors merging of strips and minimal interfaces. States with backward tilting strips offers an compromise: the interfaces are not quite as vertical but the strips are not too narrow. At $H = 6$, these two effects compete constantly, leading to a combination of $\tan\theta \sim 6/36$ and $\tan\theta \backsim -2/26$ strips, which we call a hybrid. As observed, such states survive to rather low temperatures. By contrast, we saw in Chapter

5 that the $\Omega = 4$ state for $H = 18$, being aligned with the field, survives up to $T \backsim 1.3$.

Turning to runs with lower densities, we plot the time traces for two systems at $T = 0.8, 0.7$ and 0.5. While establishing the co-existence curve, we noticed that, in the less dense systems, there are not have enough particles to support the hybrid state, with backward tilted clusters dominating the sampled configurations. Thus, we search for system with lowest critical density $\bar{\rho}_c$ for the hybrid state to exist. In Figures 6.18, we show time traces for $\bar{\rho} = 20/72$ and observe that the system is dominated by backward strips regardless of initialization. Unlike the half-filled case, this system contains fewer particles so that such states are characterized by $\Delta\rho_6 \backsim 6$ and $\Delta\rho_{-2} \gtrsim 8$. The traces illustrates that this "pure" state is the stable inhomogeneous state for all T. One possible explanation for the difference between this and the half-filled case is that, with fewer particles overall, the droplet-like strip are more localized and less likely to interact with itself (through SPBC and multiple winding) in a way that promotes aggregation into hybrid structures.. Similarly, once a thick strip is formed, the field is more effective in dividing it if there are fewer particles in the hole-rich region. Above $T = 0.8$, this system disorders whereas the half-filled system forms a hybrid state.

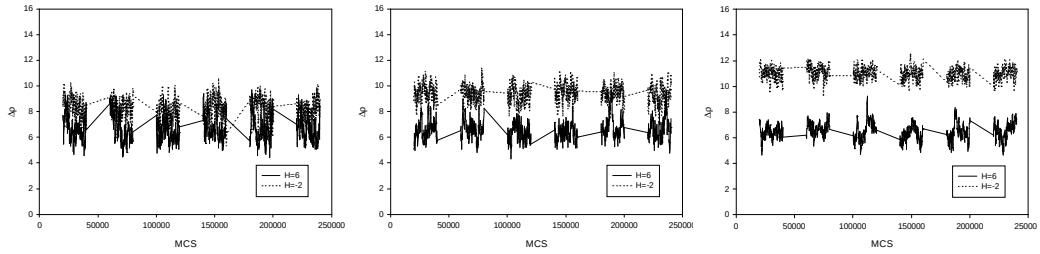

(a) T=0.8 (b) T=0.7 (c) T=0.5

Figure 6.18 Time traces of $\Delta\rho_6$ and $\Delta\rho_{-2}$ for $\bar{\rho} = 20/72$

At a slightly higher density, $\bar{\rho} = 26/72$, thresholds of hybrid states emerge. For example, on the left edge of the large cluster in Figure 6.10b, we see the signs of strip-merging, a process which leads to a hybrid state like that in Figure 6.10c. This type of "flirting" with the hybrid state can also be seen in Figures 6.19, the time traces of $\Delta\rho_6$ and $\Delta\rho_{-2}$. Even at the lowest T, we see that the system finds itself briefly in a hybrid state ($\Delta\rho_6 \tilde{} \Delta\rho_{-2}$). Thus, we conclude that, at this density, there is a small range of T in which the hybrid state exists, leading us to a rough estimate of critical density for the hybrid state as $\bar{\rho}_c$=$23/72 \pm 3/72$. Needless to say, much more detailed analysis is required before firm conclusions about hybrid states can be drawn.

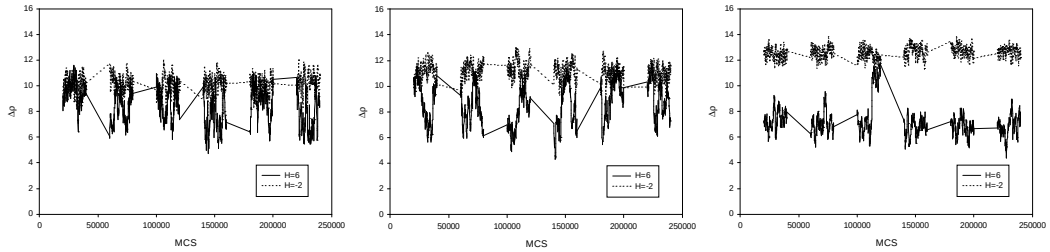

(a) T=0.8 (b) T=0.7 (c) T=0.5

Figure 6.19 Time traces of $\Delta\rho_6$ and $\Delta\rho_{-2}$ for $\bar{\rho} = 26/72$

In this chapter, we see that the $H = 6$ system deserves to be called a "critical" system, in the sense that there appeared to be extraordinarily large fluctuations. At very high temperatures or very low densities, the system is well behaved, since it is deep in the region of homogeneous states. For low temperatures and densities above some critical value, inhomogeneities appear, starting with droplet-like clusters and ending with a strip which spans the system-size. Both types of states display backward tilting structures, so that the multiple winding is given by $\Omega = 10$. We call this a "pure" state, in the sense that it closely resemble the phase separated state in equilibrium systems. Of course, there are major differences. The droplet is expected to drift with some velocity here, whereas it wanders in equilibrium case. The half-filled system contains a multiply wound strip here, as opposed to a simple strip respsecting SPBC. In both cases, we expect diffusive wandering in the strip position. However, for intermediate densities, the particle-rich and the hole-rich strips are of unequal width. In equilibrium, there is no new behavior. In contrast, we also expect the entire strip to drift. The velocity and direction of the drift is as yet to be determined.

The most interesting behavior occurs for intermediate temperatures and densities. We discovered that the system is a dynamically evolving mixture of as many as three "states": the simple single strip with $\tan\theta = 6/36$; the vertical strip; and the backward tilting domain. Lack of any better terminology, we refer to this as the hybrid state. It seems reasonable to us to think of this state as critical. However, this behavior appears to be found in a sizable region in the $\bar{\rho}$-T plane, whereas only a single point is associated with criticality in an equilibrium system. To pursue a better understanding of the co-operative properties, both dynamic and in steady state, of the system in this region is surely be a worthwhile endeavor.

7. Summary and Outlook

7.1. Summary

In this dissertation, we studied the co-operative properties of an Ising lattice gas, subjected to both an external drive and boundary conditions other than the fully periodic one (PBC). In particular, we investigated systems subjected to *shifted* periodic boundary conditions (SPBC) in *one* of the principle directions of the lattice. In the absence of a drive, such a system is not significantly different from one subjected to PBC. However, the drive takes it into a non-equilibrium steady state in a highly non-trivial manner. By placing the shift (of the SPBC) "across" the drive, we produced a competition between the two, leading to a rich variety of new phenomena.

To date, studies of co-operative behavior for driven lattice gases, above criticality, have focused mainly on systems with PBC. Likewise, studies below criticality [17] have also been performed on such systems, providing some insight into the phenomenon of phase co-existence. Only one group of authors investigated systems subjected to SPBC [15]. The original motivation for SPBC was to study interfaces that were not orientated with the drive, so that hardly any of the bulk properties in such systems are known. Since SPBC seems to have profound effects on the system as a whole, we set out to explore its effects on the co-existence curves. As a prelude, we also considered systems above T_c and established the effects of SPBC on particle correlations in the disordered phase.

Extensive Monte Carlo simulations were carried out. For high temperatures, the system is in a homogeneous, disordered phase. Here, we study particle-particle correlations, using both the standard correlation function and a newly defined, *skewed correlation function.* Contour plots of these correlations revealed that systems subjected to "low shifts" ($H \leq 4$) behave differently than those with "high shifts" ($H \geq 9$). In the former cases, the skewed correlation contours are vertical. In other words, particles form clusters that are predominantly tilted, in order to respect the SPBC. In contrast, particles in the high shift systems tend to form vertical clusters, i.e., aligned with the drive. At very high temperatures, the differences between the high and low shifted systems are less pronounced: the

correlation and skewed correlation contours are similar. Here, the distinguishing characteristic for all shifts is the well known anisotropy of the correlations near the origin.

To display large distance properties better, we measure the Fourier transforms of the these correlations, i.e., the structure factors. A well known phenomenon of driven lattice gases is that structure factors exhibit a discontinuity singularity at the origin at all temperatures above criticality, leading to generic, long range correlations. These discontinuity singularities were observed in all structure factors. Further, as a counterpart to the skewed correlation function, *skewed structure factors* were introduced. As expected, the long wavelength components of these behave much the same way as ordinary structure factors, showing discontinuity singularities and being exponentially distributed. Comparing these two kinds of structure factors is revealing. For low shifts, we infer that particles tend to cluster along the skewed direction. For high shifts, they tend to cluster along the drive direction. Structure factors were also used to show that the drive dominates at short range for all shifts and temperatures.

For systems at low temperatures in inhomogeneous states, there are macroscopic regions which are particle-rich or particle-poor. The density deep within these regions, as a function of the temperature, is known as the co-existence curve. We used two methodologies for determining such curves. Method I is based on examining directly the densities of the particle-rich and particle-poor phases in a half-filled system. Devising a reliable way to estimate these densities, we arrive at one set of co-existence curves for systems with various shifts. For the *unshifted* case, our results are consistent with those from [17]. The effects of SPBC, for low H, is to suppress ordering, so that the co-existence curves lie monotonically lower with increasing shift. In cases of large H, we find that the entire phenomenon of phase co-existence to be quite complex. First, the particle-rich region is not simply a single strip, obeying the SPBC. Instead, they break up into multiple strips. With closer examination, these are actually part of one single strip, multiply wound around the torus, in order to satisfy both the SPBC and be aligned with the drive! As a result, the ordered state in an $H = 9$ system differs from that in the $H = 18$ case. The winding number in the former system is $\Omega = 8$ so that the width of the strip is quite narrow and fluctuations can easily cause them to merge. As a result, disorder appears to set in at rather low temperatures. By contrast, $\Omega = 4$ in an $H = 18$ system, displaying wider and more stable strips, so that disorder sets in only at distinctly higher temperatures.

For an Ising system in equilibrium, another route to phase co-existence is to analyze systems with various densities $\bar{\rho}$ (i.e., different fixed magnetizations). For $T < T_c$, a system with low enough density will remain homogeneous. Only when

the density corresponding to the co-existence curve is reached will the system display inhomogeneous states. This is the basis for Method II. There are two approaches to the co-existence curve. One is to use systems with fixed $\bar{\rho} < 1/2$ and then to lower the temperature until inhomogeneities appear (or to raise T until disorder prevails). The other, more appropriate for regions where the co-existence curve has a large slope, is to fix T and vary $\bar{\rho}$ until the system shifts from one state to another. To define when a system is ordered or not, we rely on four different order parameters, as well as a series of distributions of particle densities within a column. To be sensitive to ordering in tilted states, we also measured distributions of densities in *skewed* columns. The four simple order parameters used are:

- structure factors (both ordinary and skewed) and averages over the first 9 wavenumbers
- widths of the distributions in column densities (both ordinary and skewed)
- average cluster size
- internal energy (average number of particle-hole pairs).

The general conclusion is that, at low temperatures, there is a difference between systems with low shifts and those with large shifts. In particular, ordered states for small H contain a single forward tilting strip, wound around the shifted torus in a simple manner. Systems with high H are generally found in a state with multiple winding. As for the co-existence curves, the discrepancies between Methods I and II are probably due to finite size effects in cases with low H. The discrepancies for the high shift cases are more drastic and may be largely due to fundamental differences between the inhomogeneous states in a low density system and a large density one. For example, "droplets" in the low $\bar{\rho}$ systems drift with uniform velocity, whereas the phase separated state is stationary in systems with high $\bar{\rho}$. On the whole, the co-existence curves coming from these different methods lead to a consistent picture, albeit not very accurate. In order to improve on our estimates, considerably more studies need to be carried out, as we will discuss in the next section.

Perhaps the most intriguing discovery is that, for a system with *intermediate* shift (mostly $H = 6$ in our case), there may be a substantial region in the $\bar{\rho}$-T plane in which we may use the term "critical". Extraordinarily large fluctuations are observed, tempting us to label the state as being "turbulent". The best we can conclude is that these systems appear to be in a "hybrid" state, with both forward and backward tilting strips which exchange positions and relative sizes.

It is unclear if such a state should be labelled as a steady state. To illustrate our point, we made composite figures for two typical configurations, one from an $H = 6$ system (Figure 6.1b) and the other, from an $H = 9$ study (Figure 4.4d). Instead of showing only the 72×36 lattice, we stacked these figures in accordance with the shift. The richness displayed in these figures (Figure D.5 and D.6 in Appendix D) will undoubtedly pose many interesting puzzles for some time.

7.2. Outlook

Due to the explorative nature of this dissertation, many issues and questions remain unresolved and warrant further research. We end this study with a list of possible future studies.

(i) A natural extension of our research would be to establish the co-existence curves for larger systems. Perhaps the sizes and shifts should be selected such that $\tan\theta$ remain fixed. We have stated our belief that, for small shifts, the differences in co-existence curves coming from the two methods are due to finite size effects. In particular, we expect the two estimates to converge for larger systems. For the larger shifts, we could explore the possibility that there should be two distinct curves. By collecting co-existence estimates from various system sizes, finite-scaling may be exploited so as to probe the nature of the thermodynamic limit. In a similar manner, a myriad of other studies could be performed by changing the various control parameters. For example, studies with other shifts (e.g. $H = 1, 2$ and 12) would provide a more complete description of the behavior of systems with SPBC. Investigations with smaller drives could provide new insights into the formation of multiple winding strips and the nature of the competition between the drive and SPBC. Finally, the distributions for the certain structure factors could be used as an order parameter and improve our estimation of the co-existence curve. We verified that the ordinary and skewed structure factors are distributed exponentially in the disordered state. In the ordered state, at least one of the structure factors will be well approximated by a Gaussian. A systematic catalogue of the distributions of the structure factors as a function of temperature would help expose the influence of SPBC on our system.

(ii). For systems below criticality, the nature of the interface fluctuations remains an unknown. In the unshifted system, it is known that the drive suppress interfacial roughness and gives rise to anomalous correlations [13, 29]. Given that interfacial instabilities are responsible for the *evolution* from a single to a multistrip state [30], we are certain that SPBC has a profound influence on interfaces in a steady state. The observations from our study is that, for lower shifts, coarse graining helped identify their effect on the column density distribution.

However for high shifts, the extreme roughness of the "evaporating" interface (on the right of a particle rich region, in our cases) caused serious uncertainties in this approach. Using a larger system, or perhaps with open boundary conditions, it may be possible to isolate this type of interface and its profile measured. Of course, it may hold the key to the existence and nature of the hybrid state, where "icicles" drain and break off from this interface.

(iii) For our study, $H = 6$ was a critical value. The domains and their morphologies in the different ordered states in this system could be better established with longer simulations, at various points in the $\bar{\rho}$-T plane. Similar analysis could be preformed for systems with $H = 9$. Needless to say, studies using a variety of drive strengths are needed for a better understanding of the phenomenon of the "hybrid" state.

(iv) In our study, each system is simulated by a single Monte Carlo run. Thus, we have sampled only a minute number of the possible realizations in configuration space. A collection of independent runs should be undertaken to provide better statistics. Similarly, we used a small sample of configurations in each run to estimate the co-existence curve. Longer runs will provide more accurate estimates of the curve. In the same vein, longer runs should help the system to exit the metastable states and give sharper measures of the true steady state.

(v) We have mentioned that strips in low shift, low density states drift. In a continuum theory, there is a relationship between this drift velocity and the density profile of the strip. This interesting prospect should be explored.

To conclude, this dissertation has provided a small glimpse into a system which is rather simple at the microscopic level, and yet, surprisingly complex at the macroscopic level. It shows clearly that, when driven, even the simplest models will display many interesting new phenomena. We hope that it will inspire further studies into the remarkable and unknown world of non-equilibrium statistical mechanics.

Appendix A:
Definition of $\tilde{G}$ at integer values

This appendix contains the technical details of how contour plots of $\tilde{G}$ are made. The routine we used required a square grid of points be given. However, $\tilde{G}$ is not defined on integer points in general. For convenience, we define $\tilde{G}$ on the square grid by simple interpolation. Thus,

$$\tilde{G}(i,j) \equiv (1-s)G(\left[i+\frac{H}{M}j\right],j) + sG(\left[i+\frac{H}{M}j+sgn(j)\right],j)$$

where $sgn(j)$is the sign of j , $[\cdot]$ stands for the integer part of $\cdot$ and s

$$s \;=\; i+\frac{H}{M}j-\left[i+\frac{H}{M}j\right].$$

Appendix B:
Skewed symmetry of $e^{i\bar{\mathbf{k}}\cdot\mathbf{x}}$

An ordinary plane wave $e^{i\mathbf{k}\cdot\mathbf{x}}$ is periodic in wave-vector space, so that letting n_x take integer values in $[0, L-1]$ is just as convenient as in $\left[-\frac{L}{2}, \frac{L}{2}\right]$. For the complete set

$$u(n_x, n_y) \equiv e^{i\bar{\mathbf{k}}\cdot\mathbf{x}}$$

where

$$\bar{\mathbf{k}} = (\tilde{k}_x, \tilde{k}_y) = 2\pi \left(\frac{n_x}{L}, \frac{n_y}{M} - \frac{n_x H}{LM} \right),$$

there is a slight difference. In particular, this set satisfies SPBC:

$$\begin{aligned} u(L - n_x, n_y + H) &= \exp\left[2\pi i \left(x \frac{L - n_x}{L} + y \left\{ \frac{n_y + H}{M} - \frac{(L - n_x)\, H}{LM} \right\} \right) \right] \\ &= \exp\left[2\pi i \left(\frac{-n_x x}{L} + y \left\{ \frac{n_y}{M} - \frac{-n_x H}{LM} \right\} \right) \right] \\ &= u(-n_x, n_y) \end{aligned}$$

instead of $u(L - n_x, n_y) = u(-n_x, n_y)$. As a result, we need to exercise some care in, e.g., interpretating data for $S(n_x, n_y)$ in the limited range of, say, $n_x \in [0, L-1]$ and $n_y \in [0, 1]$.

Appendix C: Example of S and $\tilde{S}$ for different ordered states

As an example we compute the transforms, in the continuum limit, for a strip of width w, wrapped around a torus with SPBC in a continuous manner. Using orthogonal co-ordinates (x, y), this configuration is given simply by

$$n(x,y) = \Theta\left\{x - \lambda y\right\}\Theta\left\{w - x + \lambda y\right\},$$

where Θ is the standard step function and

$$\lambda \equiv H/M.$$

Note that, for convenience, we are using the density, rather than the spin, variable.

Then, to obatain the ordinary structure factor, for which $k_x = 2\pi n_x/L$ and $k_y = 2\pi n_y/M$, we compute

$$f(n_x,n_y) = \frac{1}{LM}\int_{\mathbf{0}}^{M} e^{ik_y y}dy \int_{\lambda y}^{w+\lambda y} e^{ik_x x}dx = \frac{(e^{i2\pi w n_x/L}-1)}{2\pi i n_x}\frac{(e^{i2\pi\left(n_y+\frac{H}{L}n_x\right)}-1)}{2\pi i(n_y+\frac{H}{L}n_x)}$$

so that

$$S(n_x,n_y) = \frac{\left[1-\cos\left(2\pi w n_x/L\right)\right]\left[1-\cos\left(2\pi H n_x/L\right)\right]}{4\pi^4 n_x^2\left(n_y + H n_x/L\right)^2}.$$

Note that this formula is not valid for the special case $n_y = H = 0$.

By contrast, for the skewed structure factor, for which

$$(\tilde{k}_x,\tilde{k}_y) = 2\pi\left(\frac{n_x}{L}, \frac{n_y}{M} - \frac{n_x H}{LM}\right),$$

we have

$$\tilde{f}(n_x,n_y) = \frac{1}{LM}\int_{\mathbf{0}}^{M} e^{i\tilde{k}_y y}dy \int_{\lambda y}^{w+\lambda y} e^{i\tilde{k}_x x}dx = \frac{(e^{i2\pi w n_x/L}-1)}{2\pi i n_x}\delta_{\mathbf{0},n_y}$$

so that the simple form

$$\tilde{S}_H(n_x, n_y) = \frac{[1 - \cos(2\pi w n_x/L)]\,\delta_{0,n_y}}{2\pi^2 n_x^2}$$

is recovered. Of course, in the special case of $w = L/2$, this reduces to the usual: $\tilde{S} = 0$ except for $n_y = 0$ and odd n_x, when it is

$$\tilde{S}_H(n_x, n_y) = \frac{1}{\pi^2 n_x^2}.$$

Note that this is a good approximation for small (n_x, n_y). In the simulations, a finite lattice is used, so that the interfaces of such a tilted ordered strip will consists of steps and "terraces". An example is shown in Fig. C.1 for the $H = 4$ case.

Figure C.1 A half-filled, ordered state with $H = 4$

Then the density function will read

$$n(x, y) = \Theta\{x - [\lambda y]\}\,\Theta\{[w + \lambda y] - x\},$$

where $[\cdot]$ stands for the integer part of $\cdot$, with the result that $\tilde{S}_H(n_x, n_y)$ will be somewhat more complicated than stated above. In Table A.1, we show both S and $\tilde{S}$ obtained from the configuration in Fig A.1, for the first few (n_x, n_y). It clearly demonstrates that, unlike the ordinary structure factor, $\tilde{S}$ is concentrated in $n_y = 0$ and decays roughly as n_x^{-2}.

$n_y \backslash\ n_x$	1	3	5	7	9
0	1044	108	33	14	6
1	3	2	2	1	1
2	1	1	0	0	0

Table A.1(a) The ordinary structure factor for the ordered state in Fig. A.1

$n_y \backslash\ n_x$	1	3	5	7	9
0	1051	117	42	21	130
1	0	0	0	0	0
2	0	0	0	0	0

Table A.1(b) The skewed structure factor $\tilde{S}_4$ for the ordered state in Fig. A.1

Appendix D:
Cluster Distributions and Configurations

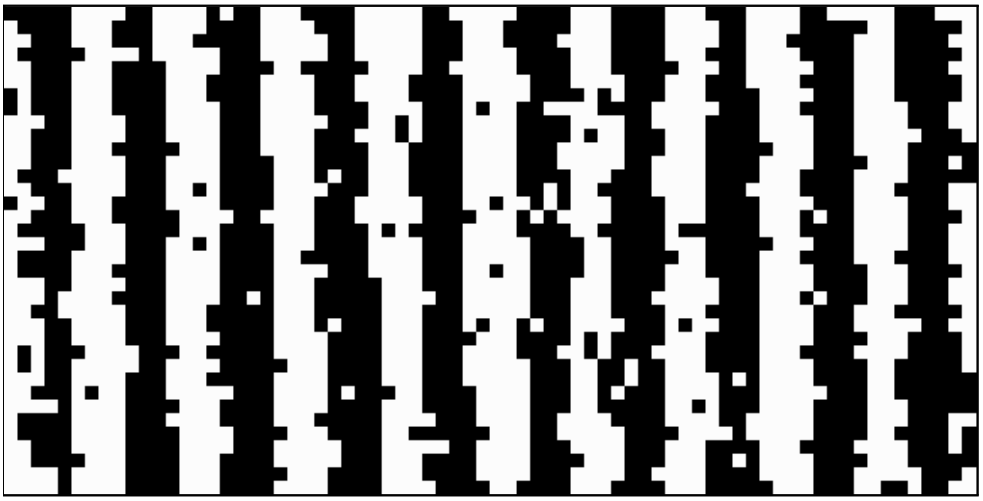

Figure D.1 Backward tilting multiple windings: H=6, T=0.7 (Chapter 4,6)

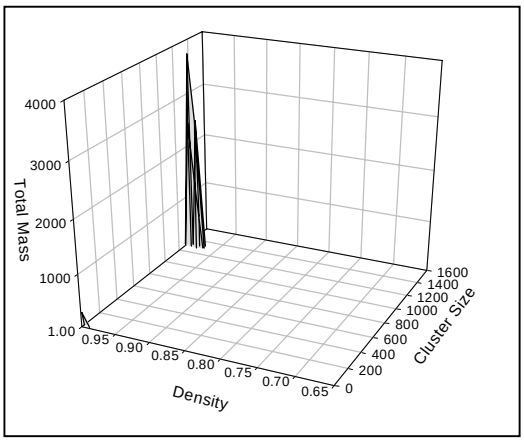

(a) T=0.8

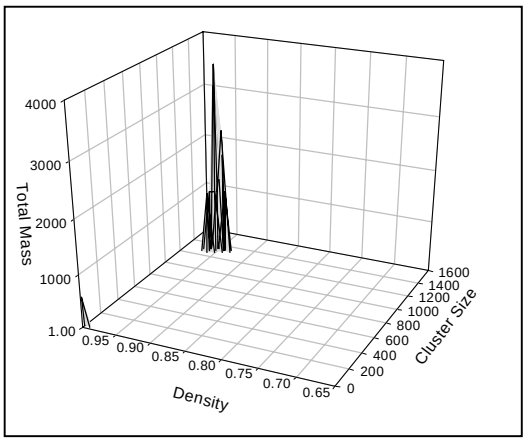

(b) T=1.0

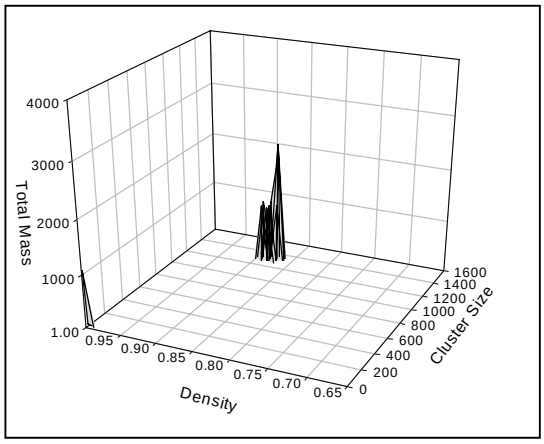

(c) T=1.2

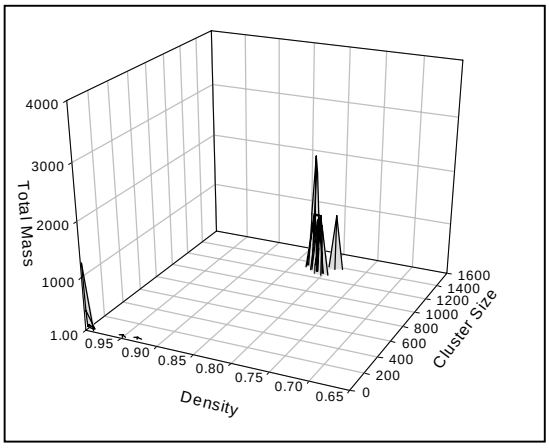

(d) T=1.3

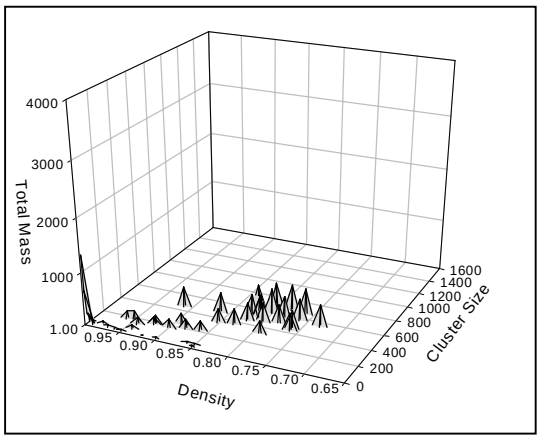

(e) T=1.4

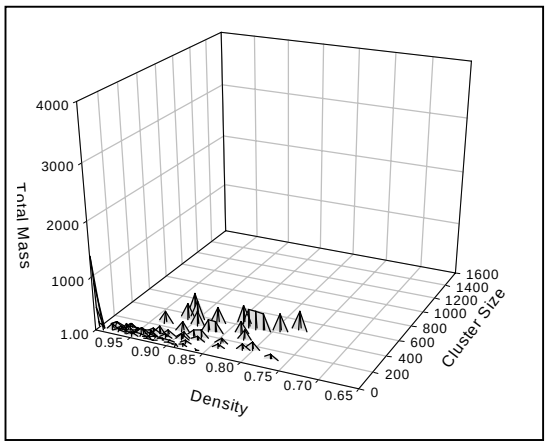

(f) T=1.8

Figure D.2 Cluster Distributions: H=0, ρ=36/72 (Chapter 5)

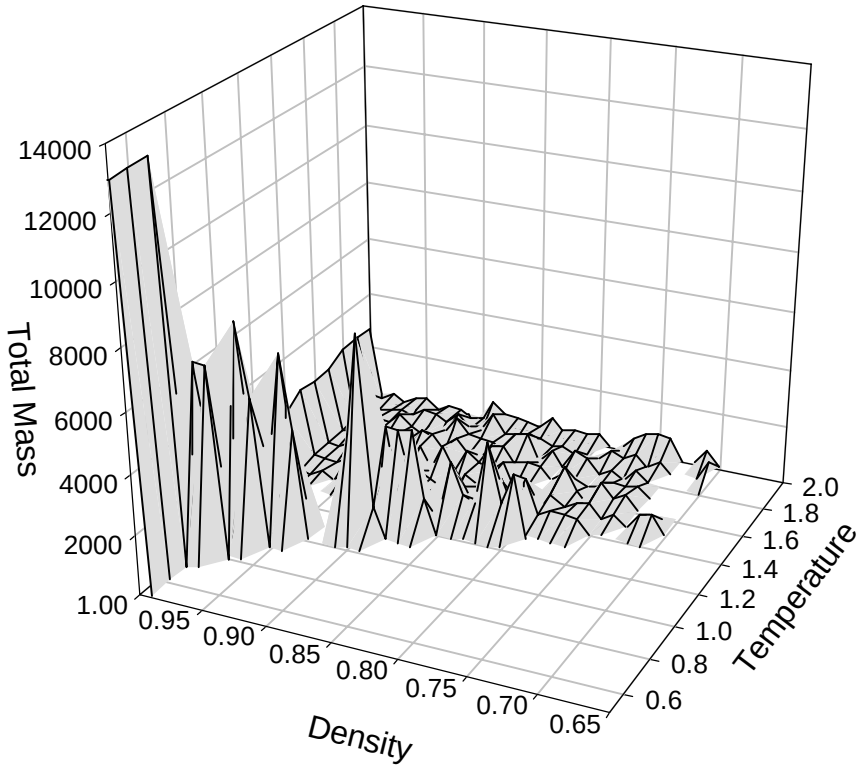

Figure D.3 Mass Distribution in the $\overline{\rho}_{clus}$-T plane for the H=0, $\overline{\rho}$ =36/72 (Chapter 5)

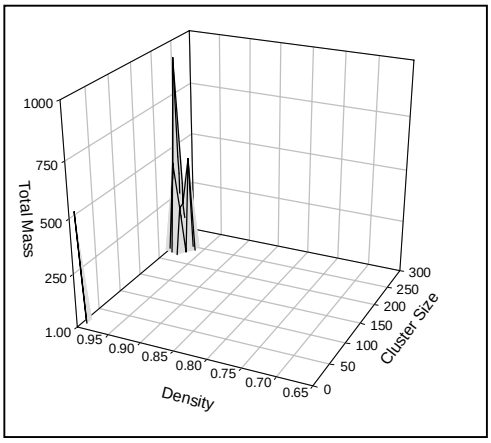

(a) T=0.8 Heating

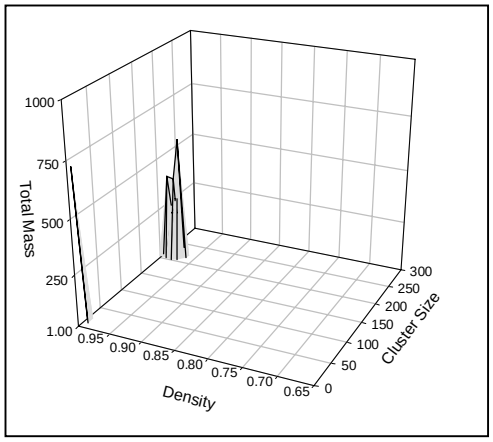

(b) T=0.9 Heating

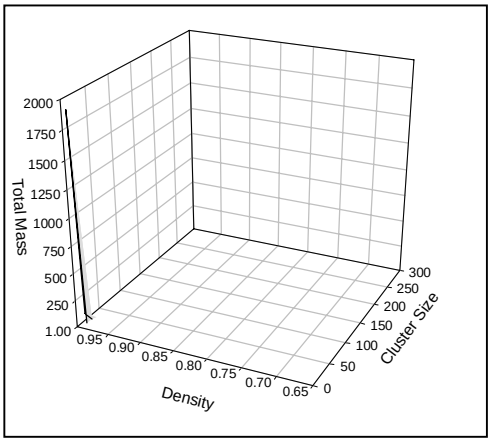

(c) T=1.0 Heating

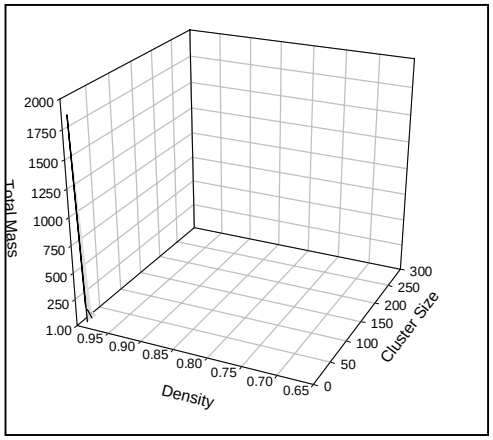

(d) T=0.9 Cooling

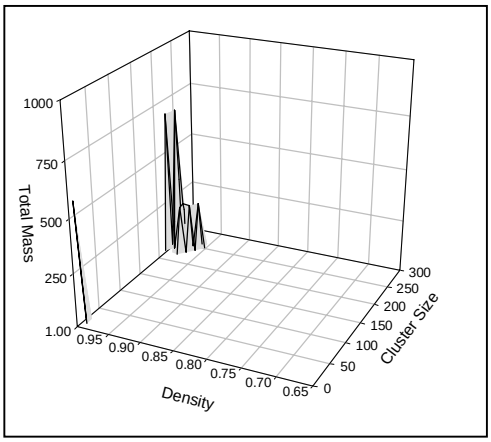

(e) T=0.8 Cooling

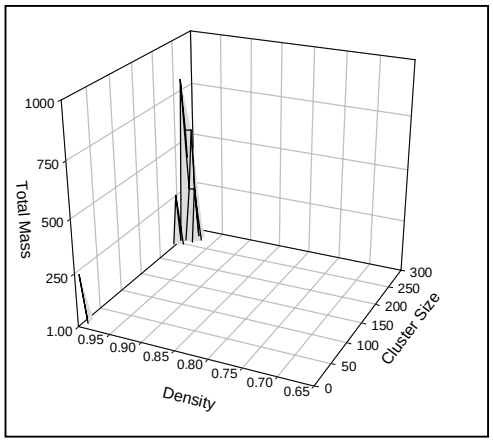

(f) T=0.7 Cooling

Figure D.4 Cluster Distributions for H=0, ρ=8/72 (Chapter 5)

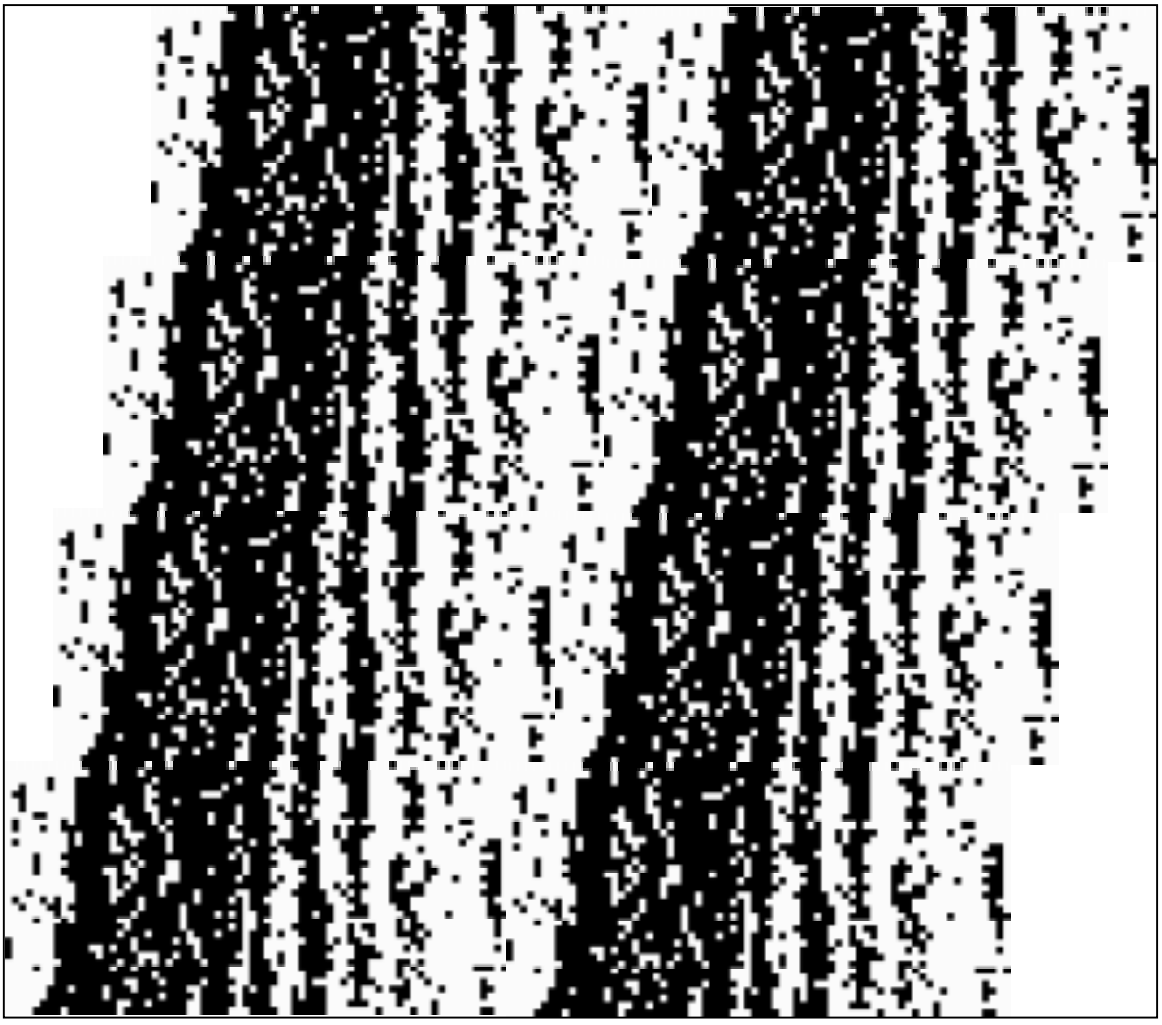

Figure D.5 H=6 "Hybrid" State at T=0.8 in the Heating Cycle (Chapter 7)

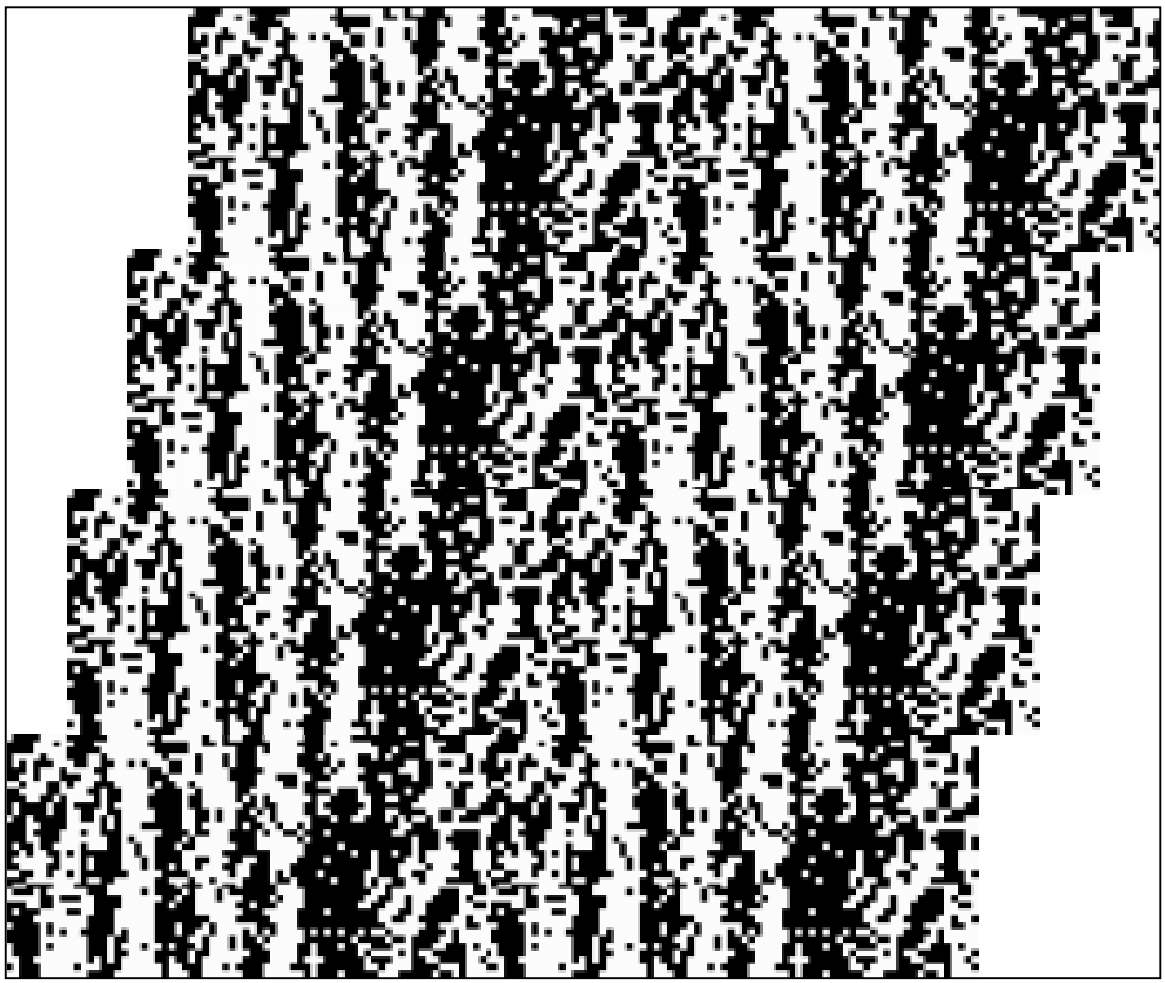

Figure D.6 H=9 "Hybrid" State at T=1.1 in the Cooling Cycle (Chapter 7)

Bibliography

[1] J.W. Gibbs, *The Elementary Principles in Statistical Mechanics.* (Scribner, NY 1902).

[2] S. Katz, J.L. Lebowitz and H. Spohn, *Phys. Rev. B* **28** 1655 (1983) and *J. Stat. Phys.* **34** 497 (1984) .

[3] B. Schmittmann and R.K.P. Zia, in: *Phase Transitions and Critical Phenomena*, Vol. 17, C. Domb and J.L. Lebowitz, eds. (Academic Press, London, 1995).

[4] S. Chandra, *Superionic Solids. Principles and Applications.* (North Holland, Amsterdam 1981).

[5] Ising, Z. Physik **31** 253 (1925).

[6] C.N. Yang and T.D. Lee, Phys. Rev. **87** 404 (1952); and T.D. Lee and C.N. Yang, Phys. Rev. **87** 410 (1952).

[7] L. Onsager, *Phys. Rev.* 65 117 (1944).

[8] B. M. McCoy and T. T. Wu, *The Two-dimensional Ising Model.* (Harvard Univ. Press, Cambridge, Mass., 1973)

[9] C.N. Yang, *Phys. Rev.* 85 808 (1952).

[10] K.G. Wilson and M.E. Fisher, *Phys. Rev. Lett.* **28** 240 (1972).

[11] R.J. Glauber, *J. Math. Phys.* **4** 294 (1963).

[12] K. Kawasaki, *Phys. Rev.* **148** 375 (1966).

[13] K.-t. Leung, K. K. Mon, J. L. Valles and R. K. P. Zia, Physical Review Letters 61 1744 (1988) and K.-t. Leung, K. K. Mon, J. L. Vallés and R. K. P. Zia, Physical Review B39 9312-9317 (1989).

[14] See references in, e.g., R.K.P. Zia, in *Statistical and Particle Physics: Common Problems and Techniques*, eds. K.C. Bowler and A.J. McKane (SUSSP Publications, Edindburg, 1984).

[15] J. L. Vallés, K.-t. Leung and R.K.P. Zia, *J. Stat. Phys.* **56** 43 (1989).

[16] J. Marro and J.L.Vallés, *J. Stat. Phys.* **49** 121 (1987).

[17] J.L. Vallés and J. Marro, *J. Stat. Phys.* **56** 43 (1987).

[18] K.-t. Leung and R.K.P. Zia, *J. Phys. A* **23** 4593 (1990).

[19] K.-t. Leung and R.K.P. Zia, *Phys. Rev. E* **56** 308 (1997).

[20] N. Metropolis, A.W. Rosenbluth, M.M. Rosenbluth, A.H. Teller and E. Teller, *J. Chem. Phys.* **21** 1087 (1953).

[21] M.Q. Zhang, *Phys. Rev.* **A35** 2266 (1987).

[22] R. K. P. Zia and T. Blum, in *Scale Invariance, Interfaces and Non-equilibrium Dynamics*, eds. M.Droz, A.J.McKane, J.Vannimenus and D.E.Wolf (Plenum,NY,1995).

[23] M.Q. Zhang, J.-S. Wang, J.L. Lebowitz and J.L. Valles, *J. Stat. Phys.* **52** 1461 (1988).

[24] R.K.P. Zia, K. Hwang, B. Schmittmann and K.-t. Leung, *Physica A* **194** 183 (1993).

[25] H.K. Janssen and B. Schmittmann, *Z. Phys. B* **64** 503 (1986); K.-t. Leung and J.L. Cardy, *J. Stat. Phys.* **44** 567 (1986) and **45** 1087 (1986).

[26] K.-t. Leung, *Phys. Rev. Lett.* **66** 453 (1991) and *Int. J. Mod. Phys. C* **3**: 367 (1992); J.-S. Wang, *J. Stat. Phys.* **82**: 1409 (1996).

[27] K.K. Mon, S. Wahsleben, D.P. Landau, and K. Binder, *Phys. Rev. Lett.* **60** 708 (1988)

[28] F. P. Buff, R. A. Lovett and F. H. Stillinger, *Phys. Rev. Lett.*, **15** 621 (1965); B. Widom and J.S. Rowlinson, *Molecular Theory of Capillarity* (Oxford, 1982).

[29] K.-t. Leung and R.K.P. Zia, *J. Phys. A* **26** L737 (1993).

[30] K.-t. Leung, *J. Stat. Phys.* **61** 341 (1990).

[31] Rudzinsky and Zia, *J. Phys. A* **29** 6717 (1996).

[32] K. Binder, *Monte Carlo Methods in Statistical Physics I* (Spring, Berlin, 1979).

[33] L. P. Kadanoff, *Physics* **2** 263 (1966).

VITA

Birthdate/Place :	August 14, 1964; Quebec, Canada
Marital Status :	married, May 21, 1988
Children:	Matthew (born: August 28, 1993)
	Scott (born: July 17, 1995)
Education:	
1987	B.Sc. Engineering Physics at University of Colorado
1995	M.Sc. at Virginia Polytechnic Institute & State University
1998	Ph.D. at Virginia Polytechnic Institute & State University
Experience :	
1987-	Employed at NSWCDD, Dahlgren, V.A.

Research Interest:

- Non-equilibrium statistical mechanics
- Driven-diffusive systems
- Monte-Carlo simulation techniques
- Estimation Theory
- Geodesy